

Copyright 2005 Society of Photo-Optical Instrumentation Engineers.

This paper was (will be) published in [add journal or proceedings bibliographic information] and is made available as an electronic reprint (preprint) with permission of SPIE. One print or electronic copy may be made for personal use only. Systematic or multiple reproduction, distribution to multiple locations via electronic or other means, duplication of any material in this paper for a fee or for commercial purposes, or modification of the content of the paper are prohibited.

An Integrated Imaging System for the 45-nm Technology Node Contact Holes Using Polarized OAI, Immersion, Weak PSM, and Negative Resists

John S. Petersen, Mark J. Maslow, Robert T. Greenway

Petersen Advanced Lithography, Inc., 12325 Hymeadow Drive, Suite 2-201

Austin, TX 78750, www.advlitho.com, jpetersen@advlitho.com

Abstract

Imaging contact holes has become a major technology barrier for optical lithography in the deep sub-wavelength era. Using hyper-numerical aperture, extreme off-axis illumination with TE-polarization, weak PSM and negative-acting resists 50nm contacts on a 90nm pitch can be produced with better than 0.3 micron depth-of-focus with 5% exposure latitude and maximum exposure latitude of greater than 15% at best focus. Large depth-of-focus across-pitch range solutions for 50nm contacts require the use of multiple exposures using unique sources but smaller focus budgets can be reduced to single exposure. This work defines possible integrated imaging systems that will allow imaging of deep sub-wavelength sized contact holes and then compares these to other solutions that have been proposed in the literature. Specifically, source design through normalized-image-log-slope, normalized-resist-image-log-slope and process window mapping, development of contact hole primitives using full mask transform correction (where the mask pattern shape, material and topography are taken into account) and resist requirements will be discussed for developing dense, mid-range and isolated pitch contact hole imaging solutions for the 45nm technology node.

Keywords: 45nm, negative resists; immersion lithography, polarization, PSM, OAI, vortex, CPL

Introduction

Starting with the 130nm technology node, resolving contact holes is the primary feature size and pitch limiter. Relative to lines and spaces the normalized-image-log-slope (NILS) and intensity maximum of the projected image are significantly worse for contacts imaged in positive-tone resists. Our work shows NILS of less than 1.5 is typical for 160nm pitches imaged with 0.75 NA 193nm and c-Quasar. This is due in large part to the loss in cross term diffraction information that is filtered by the pupil reducing both contrast and intensity and that is then compensated by increasing the size of the contact and sampling the low NILS region near the intensity maximum to attain sizing through underexposure. It is also due to the type of off-axis illumination scheme used to attain the small pitch. Using an off-axis illuminator poles placed at the 45 degree position relative to the optical axis limits resolution to a pitch factor of $1/\sqrt{2}$ whereas with the poles oriented on the optical axis resolution can extend to $1/2$. However, while increasing resolution, this is done at a loss to contrast due to two poles being ideally oriented to form good diffraction information for each x-orientation or y-orientation feature edge while the other two are not.¹ This problem can be mitigated by using y-polarization for x-edge and x-polarization for each y-edge in a dual dipole exposure or by using azimuthally polarized source in a single exposure.² Yet after doing this, the lithographer is still faced with the problems inherent with underexposing low contrast images, poor process latitude and a greater propensity for line-edge-roughness in positive resist.

Using negative-tone resists may offer several viable alternative solutions for improving the lithographic potential to image contacts and to extend their resolution to the smaller pitches.^{3, 4} The oldest of the methods discussed here uses two exposures to place an x-oriented grating down in one exposure and a y-oriented grating and then a third exposure stenciling the desired array pattern by using exposure to close unwanted holes.⁵ This is expensive and won't be dealt with here. The use of negative type contacts has most recently been proposed by Levenson^{6, 7} using the Vortex contact and has been further promoted in the work of Liu⁸. This method of strong phase shifting that, while having some fairly extreme fabrication and optical-proximity correction issues, has great promise but for our work has too severe of proximity effects to be viable for our pitch range of interest. The focus-exposure process windows show this in Figure 1. This Figure represents $\pm 10\%$ CD process windows from 90nm to 180nm pitch and shows for aqueous immersion lithography simulation using dry NA of 0.95 and azimuthally polarized source that each pitch has adequate process potential stability but different sizing dose for its process window thus making it unusable without correction. While there may be more optical lithographic methods using pupil filters or maskless, this brings us to our topic, the imaging of contact holes using weak phase-shift hybrid-chromeless phase masks.

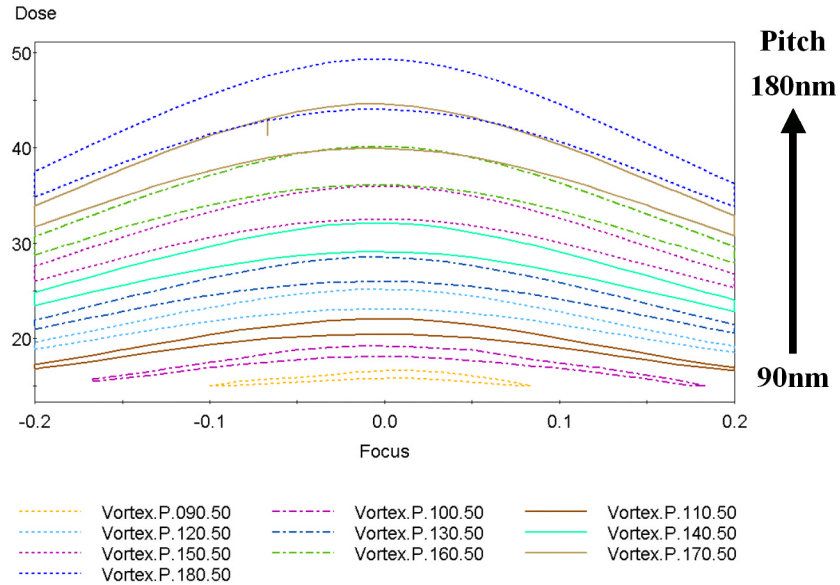


Figure 1: 50nm contact holes for pitches from 90nm to 180nm. Aqueous immersion lithography simulation using dry NA of 0.95 and azimuthally polarized source. Each pitch has adequate process potential stability but different sizing dose for its process window makes it unusable without correction.

These types of masks are showing great promise for extending resolution to the 45nm-node and beyond. Using simulation, we will use them in combination with azimuthally polarized cross illuminators to produce high contrast images that with overexposure of a properly tuned negative resist provides the potential for viable multi-pitch process windows for pitches of 90nm, 100nm, 125nm, 140nm, 170nm, 210nm and 880nm. These pitches are representative of the core primitive structures from which all pitches can be built. This image design system has NILS greater than 2 and as high as 3 to 4. More importantly, the designs keep the intensity minimum acceptably low with loss of focus and, even though it does not preclude their use, does it without the use of multiple phase angle regions.

Approach

Creating the desired contact hole image requires knowledge of the exposure tool, the feature pitch and target size, the 3D-shape of the mask after fabrication of all the features, the imaging contrast and bias of the resist for each feature and the optical properties of the wafer stack. For dense patterns, global biasing was used to shape the desired image. For the structures, two corrections were made. The first correction uses Kirchoff approximation of the mask combined with off-axis azimuthally polarized source and vector model image formation in a chemically amplified negative acting resist. The last correction uses an electromagnetic-field solver (KLA-Tencor's EMF1) to correct the already Optical Proximity Corrected (OPC) mask while keeping all other parameters and models the same. PROLITH™ version 8.1.2 and 9.0 (KLA-Tencor) and ProLE™⁹ version 3.1 (Petersen Advanced Lithography Inc.) were used to do the simulations.

The need for EMF correction is shown in Figures 2 and Figure 3. Figure 2 shows that how the phase-shift is made is important for a positive contact image. If the phase cut is made in the space between the feature (mesa-type) the contact is generally brighter and of higher contrast than if the phase shift cut is made in the primary and in either case Kirchoff simulation totally fails to comprehend image formation. Figure 3 shows the difference between for Kirchoff and Maxwell based images for a negative tone contact for 50nm contact on a 170nm Pitch. Both figures show that basing OPC decisions on Kirchoff models lead to possible failure.

Our work shows that each contact primitive-type has its own unique mask transform and it must be taken into account to avoid an expensive trial and error approach. Whether this occurs in reality would ultimately be at the mercy of the mask fabrication and exposure tool conditions. Initial experimental results for 65nm node of positive tone contacts show that the EMF correction across pitch range was eight times

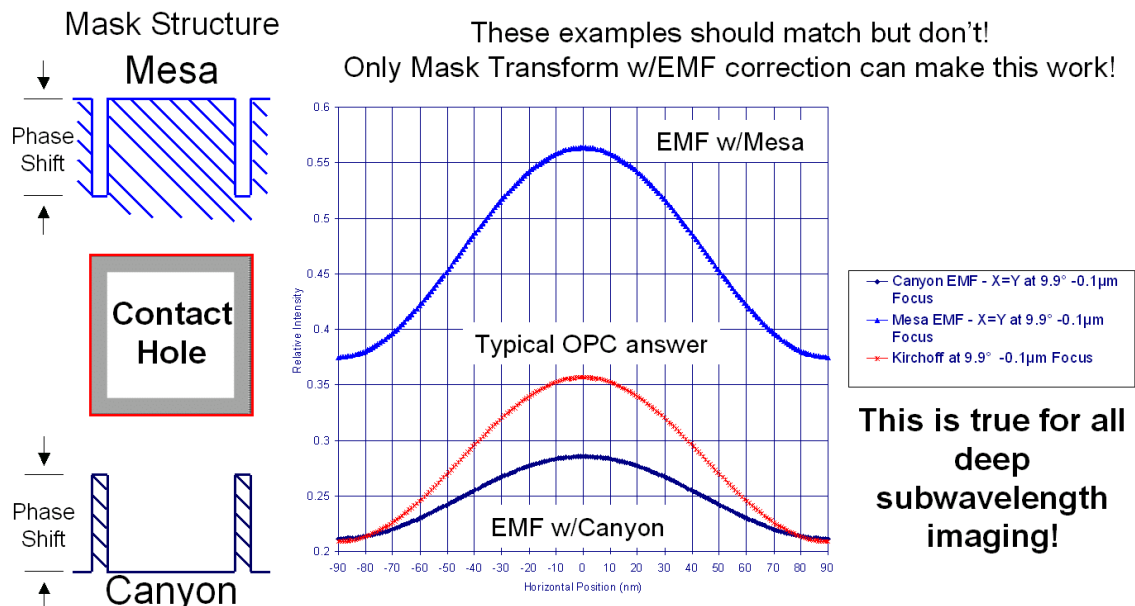


Figure 2: Aerial image comparison of different 3D mask topography that can be used to represent the same Kirchoff solution. Using a Maxwell solver it is found that neither structure matches the Kirchoff infinitely thin mask assumption. Simulation using 0.75 NA, 193nm and unpolarized c-Quasar.

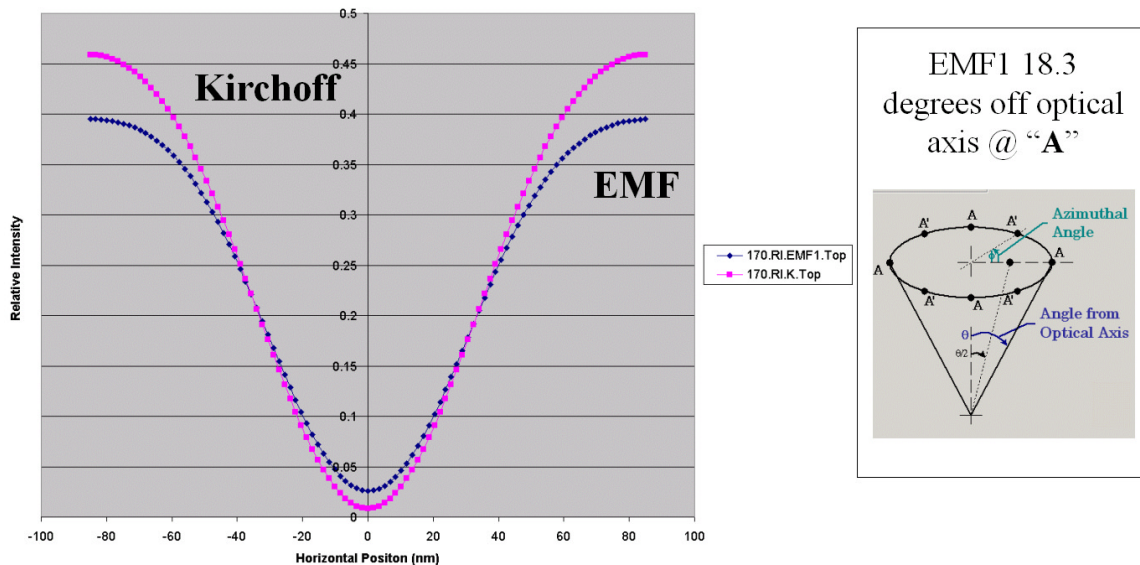


Figure 3: Aerial image of a 50nm negative contact on a 170nm pitch showing significant difference between Kirchoff and Maxwell solutions. Simulation using aqueous immersion 0.95 dry-NA, 193nm and azimuthal polarization c-Quasar.

narrower than the OPC-only range suggesting that, with proper fingerprinting of the mask and exposure tool, much tighter feature size control should be possible.¹⁰

The process of building the basic contact or contact primitive starts with isolated contacts. For isolated features, an aerial image mapping technique is used to locate side lobes and to then place assist features at those locations. Phase-shifted-clear, clear and opaque assists provide Fourier components to subtract energy from the negative contacts and to increase image contrast. Knowledge gained from EMF correction at smaller pitches is applied to larger pitch structures so that a finer simulator xyz-mesh could be used to determine the necessary corrections. Large mesh checks were made but because the object size in lithographic cases is small and does more to determine an accurate EMF-solver mesh than the wavelength (meaning that a needed 2 nm correction is not observed if the mesh is 20nm) the results were not used to make fine corrections.

Whenever possible, care is taken to match the amplitudes of the zero-order field with that of the diffraction order with the nearest symmetric-interference angle about the optical axis and to dampen others that are not symmetric.¹¹ Examples of the feature primitives are shown in Figure 2.

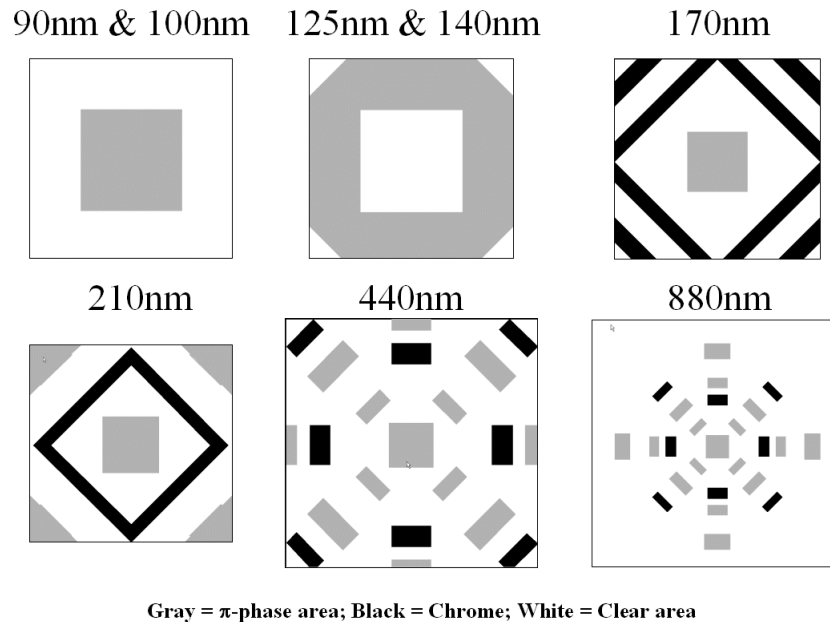


Figure 3. Examples of Kirchoff negative resist contact primitives. The dark areas are chrome, the gray areas are cut quartz phase-shifters and the clear areas are uncut quartz.

Our source design method first uses standard settings to attempt across-pitch solution. This is done by running a matrix of source settings that are constrained to $\sigma_{\text{Center}} + \sigma_{\text{Radial}} \leq \sigma_{\text{Ideal.for.90nm.Pitch}}$, then σ_{Radial} is varied about that solution in attempt to maximize the number of allowed pitches. Then for forbidden pitches we map depth of focus (DoF) of ninety symmetrically opposed $0.1 \sigma_{\text{Radial}}$ quadrupoles on a 0.1σ xy-mesh and maximize for depth of focus (DoF) using our ProLE Image Factory high performance-computing cluster.

For resist and the optical stack, we matched the index of the resist and the substrate. Figure 4 shows the transformations of an aerial image of 50nm contact on a 170nm pitch as the image forms in the resist. The responses are: image in resist at the top of the resist (square); image at the bottom (triangle); Ratio of difference top-to-bottom by bottom (X), Latent image at the resist top (*); Relative Unconverted (circle); and, on the right y-axis, the Develop clear time (seconds) (+). As the figure shows the image in the resist has less contrast than the aerial image. Further absorption was chosen to be the value of a 248nm resist like the Rohm and Haas resist UV210 and then the thickness was adjusted to provide less than 20% change in the aerial image from the top to the bottom of the resist which for this resist is 50nm. Develop

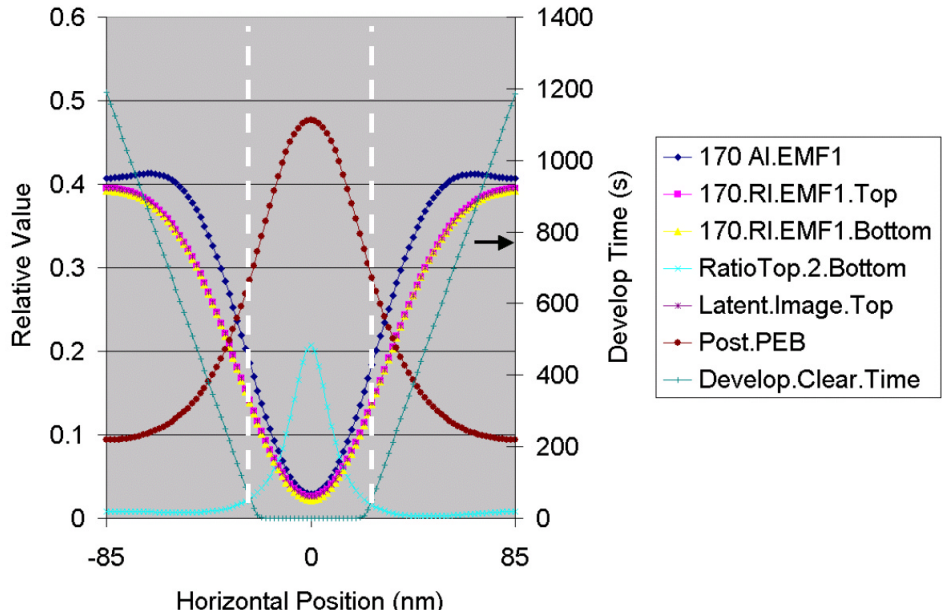


Figure 4: Transformations of an aerial image of 50nm contact on a 170nm pitch as the image forms in the resist. The responses are: image in resist at the top of the resist (square); image at the bottom (triangle); Ratio of difference top-to-bottom by bottom (X), Latent image at the resist top (*); Relative Unconverted (circle); Develop clear time (seconds) (+).

time was set to 60 seconds and will develop the post PEB image between the dotted white lines. Contrast is $n=34$ thus enough non-linear that there is little development on the outsides of the white dotted lines.

As for the rest of the simulation conditions unless otherwise stated the dry numerical aperture was 0.95 that with aqueous immersion has a numerical aperture of 1.3585. The wavelength was 193nm, with azimuthal polarization using a c-Quasar shaped illuminator. The reduction ratio was four. The resist used the UV210B resist parameters with the tone switched from positive to negative. The resist index was 1.746 and the Dill B-value was 0.35. EMF1 simulation was used with simulation at 18.3 degrees and 9.15 degrees simulated at four places the x-, y- optical axes for each angle.

Results and Discussion

Prior to starting the integration the imaging potential of a 90nm pitch and 150nm pitch was simulated using a 0.85 NA dry/1.322 NA wet and negative resist and using an optimized cross-quadrupole of σ_{Center} of 0.811 for the 90nm pitch and 0.487 for the 150nm pitch and σ_{Radial} of 0.15 for both. The primitives used were made with simple biasing. The results are shown in Figure 5. These results show that for a 5% exposure latitude the DoF is 660nm and 1000nm for the 90nm and 150nm pitches respectively.

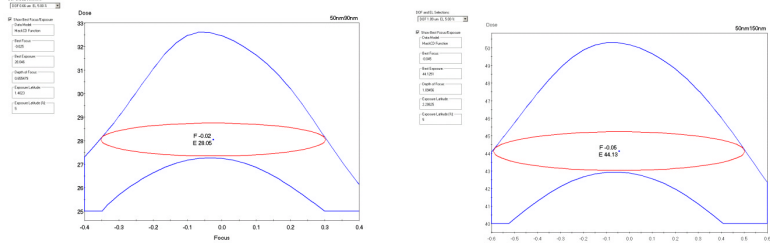


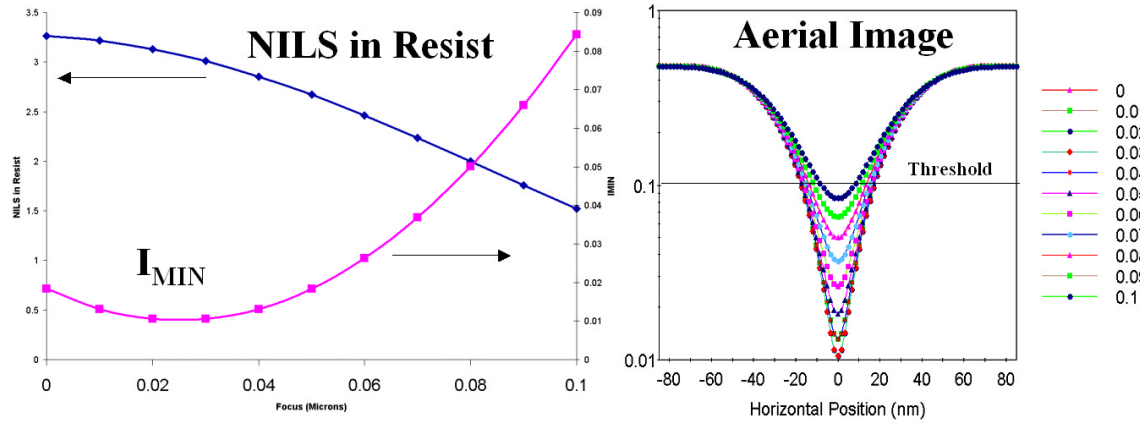
Figure 5: DoF for 90nm and 150nm pitch, 50nm contacts using an ideal source for the 90nm pitch feature

90nm Pitch w/660nm DoF

150nm Pitch w/1000nm DoF

0.85 NA dry/1.322 NA wet and negative resist

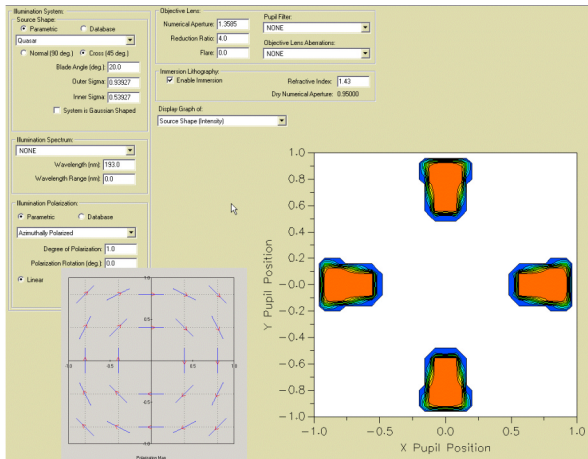
These results suggest that negative contacts have large NILS that give rise to the large exposure latitude [potential]. The failure mechanism is similar but opposite of that for positive contacts. In positive contacts loss of the intensity maximum is the key symptom to image failure and is a result of non-optimal interference of the diffraction beams with defocus.¹² However to achieve these excellent results requires multiple-exposures each with an optimal source. Analogous, for negative contacts failure is due primarily to loss of the intensity minimum and the resultant rapid change in image CD. In figure 6 the left graph shows that the NILS shift from 3.2 to 1.5 with 100nm defocus and the minimum intensity increases from 0.015 to 0.085. The right graph in Figure 6 shows the change in the intensity minimum and image CD of the aerial image keying off the 0.1 intensity threshold.



Driven by Image CD close to I_{Min}

Figure 6: The left graph shows that the NILS shift from 3.2 to 1.5 with 100nm defocus and the minimum intensity increases from 0.015 to 0.085. The right graph shows the change in the intensity minimum and image CD of the aerial image keying off the 0.1 intensity threshold.

Next as discussed in the approach we attempted to develop across-pitch solution. Since we used the ideal sigma setting of the c-Quasar for the 90nm pitch to build the contact primitives we decided to first optimize the standard illuminator. Starting with the optimal center sigma of 0.79927 as an upper constraint we varied the center sigma and the inner sigma of the c-Quasar such that the outer setting was always 0.79927. Using 70nm DoF as a process constraint and targeting 100nm DoF we found the center sigma of 0.72927 with a ± 0.2 sigma for the inner outer sigma limits and a blade setting of 20 degrees meets our goals providing we exclude a forbidden pitch. This configuration is shown in Figure 7.



PROLITH™ 9.0
(KLA-Tencor)

Illumination
90nm pitch ideal is
centered at:
0.79927 sigma

Across Pitch at:
0.73927 sigma

Figure 7: The diagram shows the exposure tool setup for the 50nm contact hole cross-pitch solution.

The results of the source depicted in Figure 7 are shown in Figures 8 and 9. For all the pitches examined Figure 8 shows focus-exposure process windows for the Kirchoff solution. This Figure shows that the common process corridor is limited by the 50nm DoF 125nm forbidden pitch. Which is further illustrated in the exposure latitude versus DoF curves shown in Figure 9. Figure 10 shows that deleting the forbidden pitch then a marginally acceptable process is obtained by increasing the DoF at 5% exposure latitude from 50nm to 90nm.

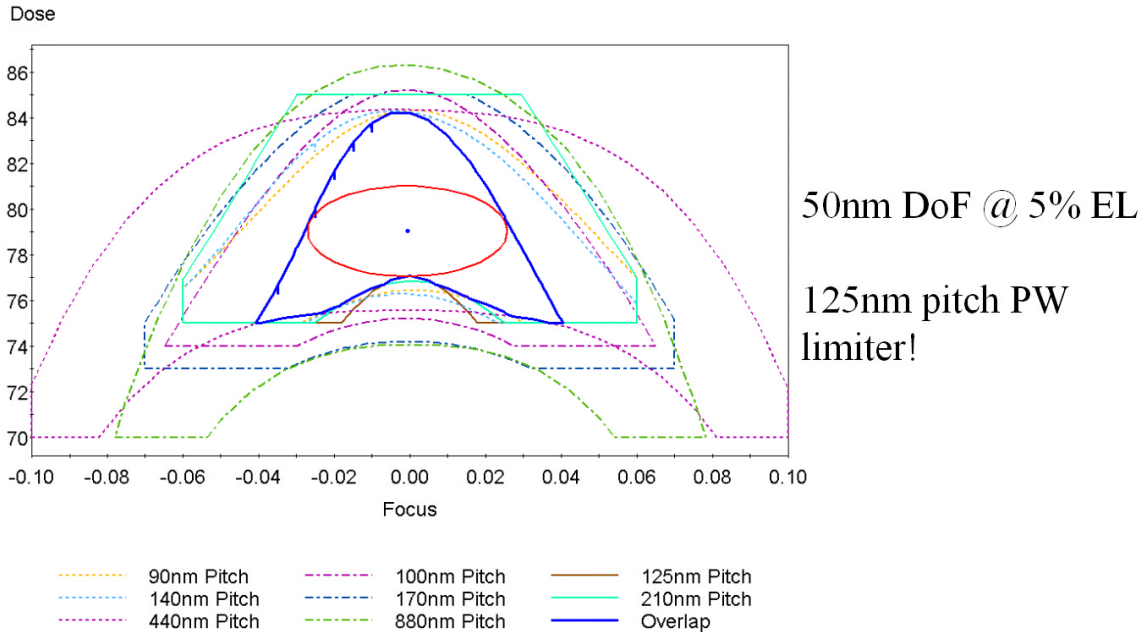


Figure 8: Focus-exposure process windows for the Kirchoff solution for all the pitches examined. The common process corridor is limited by the 125nm forbidden pitch.

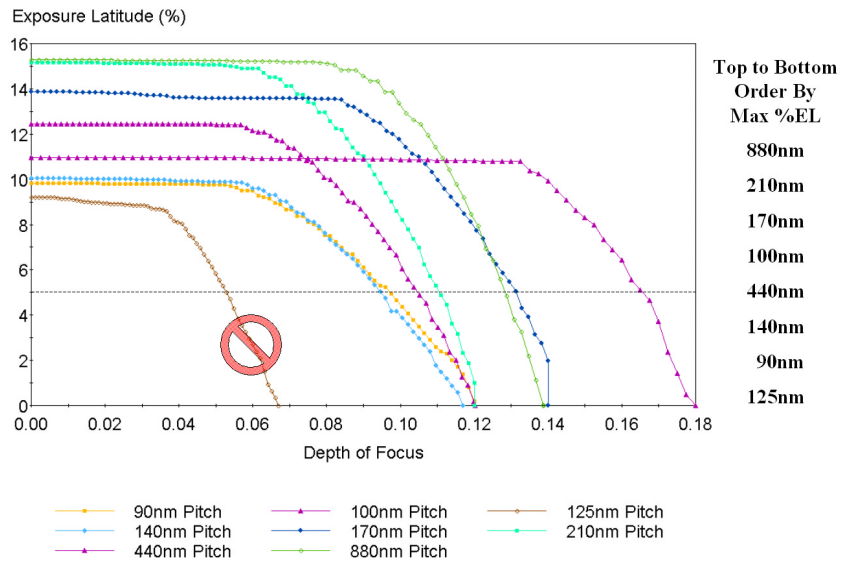


Figure 9: % Exposure Latitude versus DoF for Figure 8 process windows.

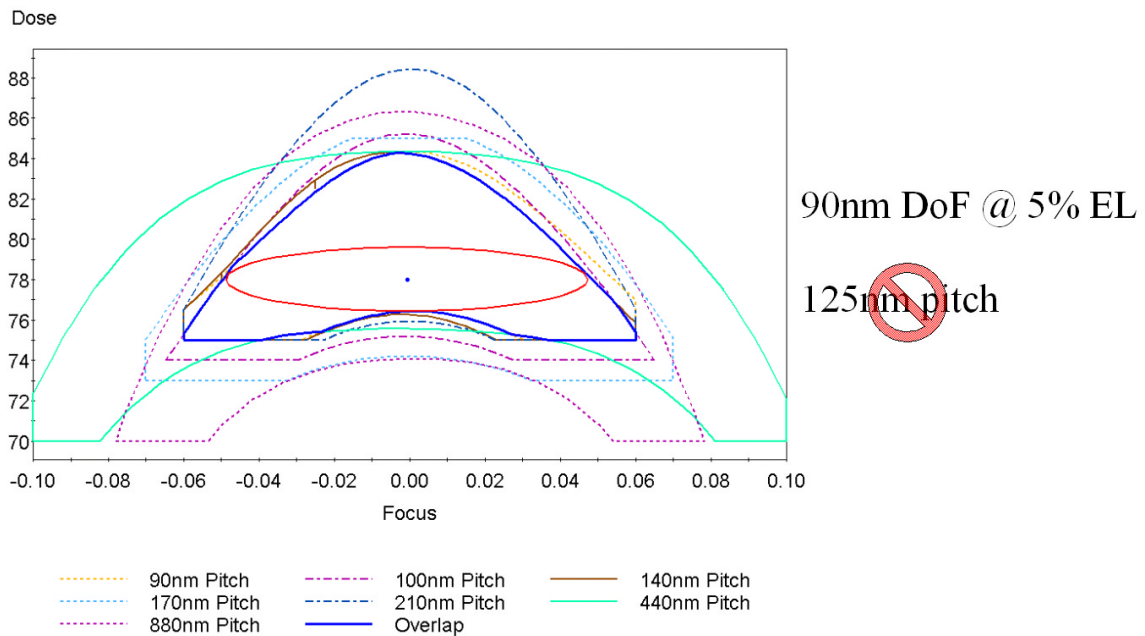
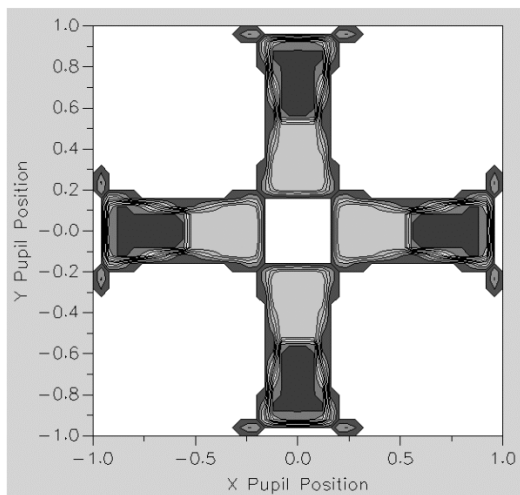


Figure 10: Re-graph of Figure 8 minus the 125nm process window. The common corridor at 5% exposure latitude increases from 50nm to 90nm.

While in this case probably the 125nm pitch would be deleted from the design rules, it will be used as tutorial for optimizing the source for a second exposure. First the pitch fails because of the non-optimal position relative to the optical axis of the first and second (the little ear shaped diffraction orders). The diffraction pattern convolved with the non-optimal source is shown in the graph on the right in Figure 11. Comparing it to the graph on the right of the optimized source convolved with the same diffraction pattern shows better symmetry than the non-optimized source depicted on the left.

**w/Source for Forbidden Pitch
Poor Angular Symmetry**



**w/Source for Fixed Pitch
Good Angular Symmetry**

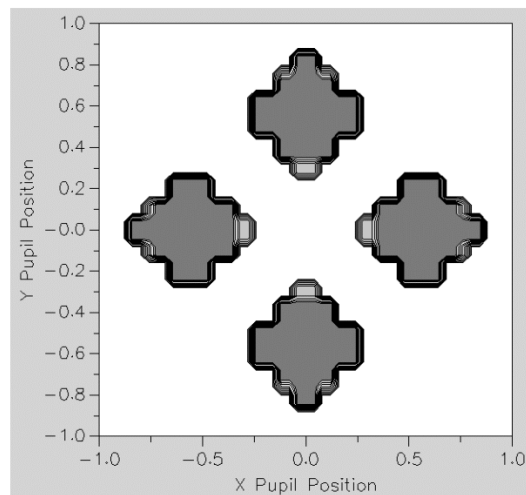


Figure 11: 125nm Pitch diffraction convolved with the source. Left graph is for the non-optimized source. Right graph is for the optimized one.

Figure 12 shows the ProLE optimized source on the left and the exposure latitude versus DoF on the right. The optimizer was set for a target range of 80nm to 160nm DoF and the result was 120nm DoF. It is not surprising the shape shows its c-Quasar lineage since the 125nm pitch primitive was originally designed for the c-Quasar.

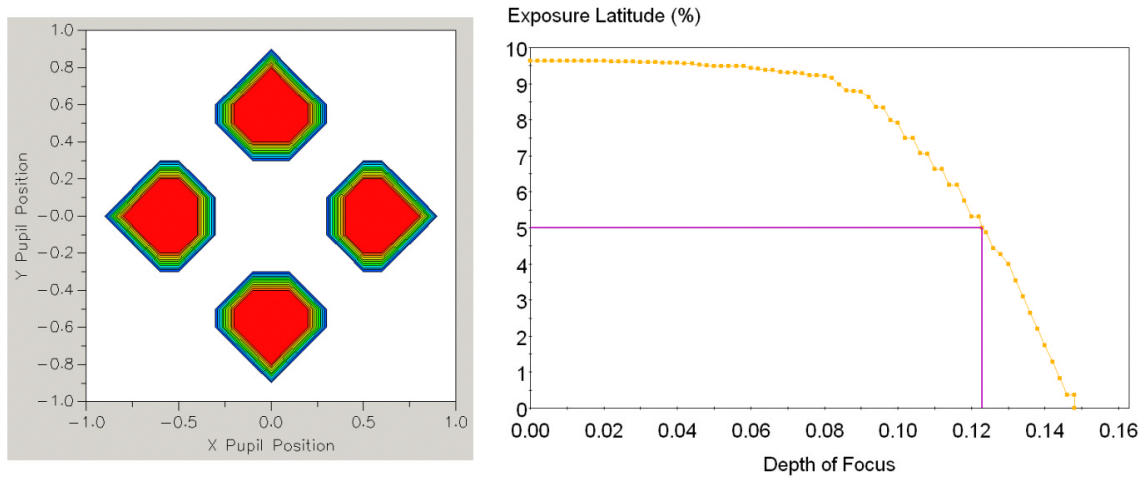


Figure 12: 125nm Pitch DoF with an Optimized Source for 2nd Exposure has 120nm DoF.

Due to the large NILS, extreme overexposure and the balancing of the magnitude of the interfering beams of the diffraction orders a lower more useable MEEF occurs. This is illustrated in Figure 13. This figure depicts the Kirchoff simulation of the overlapping focus-exposure process windows for $\pm 1\text{nm}$ mask size change of the central primary feature for the 80nm, 170nm and 210nm pitches. As expected from Figure 9 the 90nm pitch shows the greatest loss of common corridor but the overall DoF is acceptable.

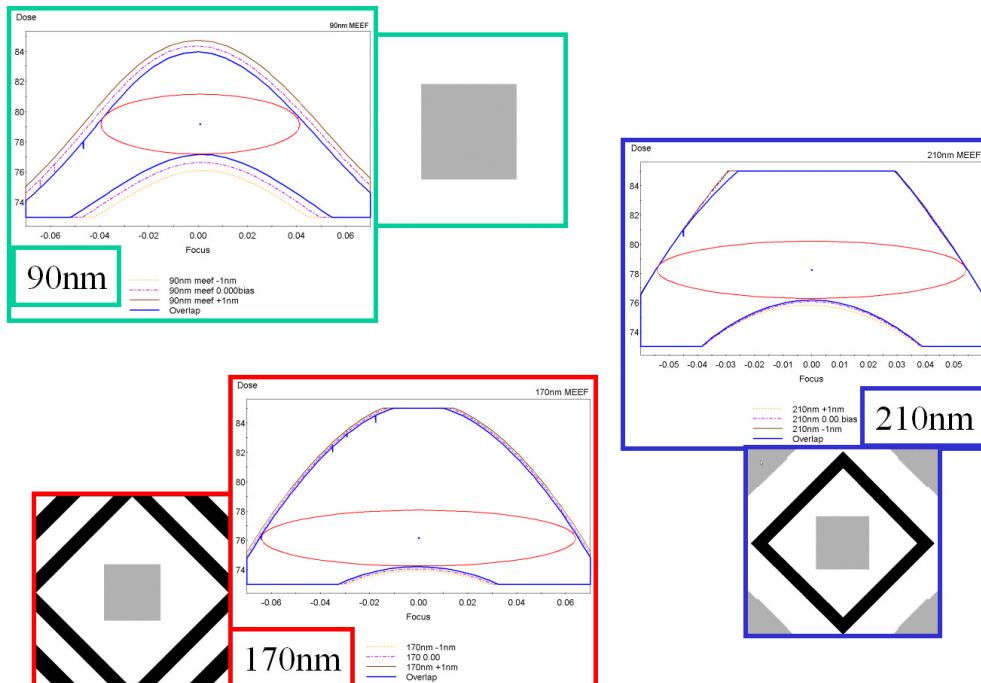


Figure 13: MEEF process window study for 50nm negative resist contacts on pitches of 90nm, 170nm and 210nm for $\pm 1\text{nm}$ mask dimension change in the primary feature.

Conclusion

Using negative resists with immersion lithography, azimuthally polarized off axis illumination and hybrid chromeless masks will make it possible to image 50nm contact holes with pitches as small as 90nm with greater latitude than their positive analogs. Kirchoff assumptions will not work and designs will need mask transform correction to be viable. The infrastructure is being built for the exposure tools and the masks but there needs to be a comparable effort to develop high resolution negative resists.

References

1. B. W. Smith, L. Zavyalova, J. S. Petersen, "Illumination pupil filtering using modified quadrupole apertures", Proc. SPIE Vol. 3334, Optical Microlithography XI; Luc Van den Hove; Ed., p. 384-394 (1998).
2. B. W. Smith, L. Zavyalova, A. Estroff, "Benefiting from polarization – effects on high-NA imaging", Proc. SPIE Vol. 5377, Optical Microlithography XVII; B. W. Smith; Ed., p. 68-79 (2004).
3. J. S. Petersen and W. Lee, "Submicron Imaging at 248.3 nm: A Lithographic Performance Review of an Advanced Negative Resist", SPIE Advances in Resist Technology and Processing, Vol. 1262, p. 358-367 (1990).
4. T. A. Brunner and C. Fonseca, "Optimum tone for various feature types: positive versus negative", Proc. SPIE Vol. 4345, Advances in Resist Technology and Processing XVIII, F. M. Houlihan, Ed., p. 30-36 (2001).
5. Y. O. Korobko, M-C. Lu, J. Telans, J. E. Powers, "Resolution limits with 248-nm strong phase-shifting techniques for contact patterning applications", Proc. SPIE Vol. 3546, 18th Annual BACUS Symposium on Photomask Technology and Management; Brian J. Grenon, Frank E. Abboud; Eds., p. 594-605 (1998).
6. M. D. Levenson, G. Dai, T. (J.) Ebihara, "The vortex mask: making 80nm Contacts with a twist!" Proc. SPIE, 4889, pp. 1293-1303, (2002).
7. M. D. Levenson, T. (J.) Ebihara, Y. Morikawa, N. Hayashi, "Vortex Via Validation", Proc. SPIE, 5256, pp. 93-102, (2004).
8. Y. Liu, J. Hu, D. Liu, "Single exposure general vortex phase-shift mask for contact hole", Proc. SPIE, 5567, pp 723-731, (2004).
9. J. S. Petersen, M. J. Maslow, Mark J., D. J. Gerold, R. T. Greenway, "Programmable lithography engine, ProLE, grid-type supercomputer and its applications", Proc. SPIE Vol. 5040, Optical Microlithography XVI; Anthony Yen; Ed. p. 1477-1491 (2003).
10. J. V. Beach, J. S. Petersen, R. T. Greenway, M. J. Maslow², S. S. MacDonald, L. H. Margolis, G. P. Hughes, "Imaging Study of Positive and Negative Tone Weak Phase-shifted 65 nm Node Contacts", Proc. SPIE, 5754, paper 5754-149 (2005).
11. "Method for phase shift mask design, fabrication, and use", US Patent 6,800,401, Date of Patent October 5, 2004.
12. R. J. Socha, J. S. Petersen, J. Fung Chen, T. L. Laidig, K. E. Wampler, R. F. Caldwell, "Design of 200-nm, 170-nm, and 140-nm DUV contact sweeper high-transmission attenuating phase-shift mask through simulation I", Proc. SPIE Vol. 3546, 18th Annual BACUS Symposium on Photomask Technology and Management; Brian J. Grenon, Frank E. Abboud; Eds., p. 617-641 (1998).